Numerical Study of Acoustic Oscillations and Combustion Instabilities in Solid Propellant Rocket

T. S. Roh*and F. E. C. Culick†
California Institute of Technology
Pasadena, CA 91125

Abstract

A numerical analysis of unsteady motions in solid rocket motors has been conducted. A fully coupled implicit scheme based on a dual time-stepping integration algorithm has been adopted to solve the governing equations and associated boundary conditions. A narrow pressure pulse is imposed at the head end to simulate unsteady acoustic oscillations in the combustion chamber. Pressure increases when the front of the pulse reaches near the nozzle area. Self-generated oscillations with frequency of standing wave propagates upstream in the combustion chamber. Investigation of transient response of gas-phase dynamics to traveling pressure wave and its effects on propellant combustion reveals several aspects: Combustion responses have a strong relationship with vorticity fluctuations in case of high turbulent intensity on the propellant surface. Temperature fluctuations of the propellant surface in the head end region seem to be very unstable and independent of the pressure wave. Surface temperature without turbulence effect looks more sensitive to temperature fluctuations in the primary flame zone. Stability of surface temperature is strongly related to turbulent intensity on the propellant surface.

Introduction

Combustion instabilities in solid propellant rocket motors have been extensively studied over several decades. Coupled interactions between combustion precesses and internal flow dynamics in chamber result in instabilities of motions in combustion chamber. Several modes of interactions between acoustic oscillations and transient combustion have been observed, the most important of which are pressure and velocity coupled responses,[1] denoting the sensitivity of combustion processes to local pressure and velocity fluctuations, respectively. Velocity coupling implies that transient combustion response is strongly influenced by the velocity oscillations parallel to the burning surface, rather than pressure oscillations.[2] Beside pressure and velocity couplings, vorticity is considered as an interaction between acoustic oscillations and transient combustion. Since combustion processes on and near the burning surface control the radial velocity, vorticity fluctuations near the propellant surface are coupled with acoustic pressure and combustion process. Vorticity fluctuations are closely related to the fluctuating radial (or vertical) velocity component upon which system stability is so strongly dependent.[3]

Various approaching methods are required to make progress in understanding mechanisms and behavior of extremely complicated combustion instabilities. Numerical simulation regarded as one of them has provided comprehensive and detailed results applicable to the real rocket motor. In a series of studies on the interactions between acoustic motions and propellant combustion,[4–8] an analysis capable of treating complicated physico-chemical processes involved in unsteady combustion of homogeneous propellants has been developed for two-dimensional Cartesian and axisymmetric combustion chambers. Turbulence closure has been achieved by means of a well-calibrated two-layer model taking into account the effect of propellant surface transport properties. It has been shown that turbulence penetrates into the primary flame zone and consequently increases the propellant burning rate, a phenomenon commonly referred to as erosive burning. The oscillatory flow characteristics are significantly altered by the turbulence due to enhanced momentum and energy transport in the gas phase. A physical insight into the gaseous dynamics and unsteady propellant

*Post-Doctoral Scholar, Mechanical Engineering and Jet Propulsion
†Professor, Mechanical Engineering and Jet Propulsion

response has been obtained from analysis of unsteady motions in the combustion chamber. There, however, is a lack of exact simulation of real motor environments because computational domains exclude the nozzle section and forced oscillations are imposed at the chamber end. Therefore, the purpose of the present work is to conduct a more complete analysis of unsteady behavior in the axisymmetric rocket motor with a nozzle. Emphasis is placed on identifying various distinct features of unsteady flow-fields of the rocket motor in oscillatory environments.

After obtaining a steady state solution, a narrow pressure pulse is imposed at the head end to obtain a natural frequency of the concerned motor and to simulate acoustic oscillations in the combustion chamber. Various aspects of interactions among traveling acoustic oscillations, unsteady reacting flows, and transient propellant combustion are investigated systematically.

Theoretical Formulation

Figure 1 shows the situation examined here, an axisymmetric rocket motor. A choked nozzle is attached to the aft end of the combustion chamber. The combustion chamber consists of the gas phase and the condensed phase loaded with a double-base homogeneous propellant grain. The analysis of the gas-phase processes is based on the complete conservation equations of mass, momentum, energy, and species concentration, and takes into account finite-rate chemical kinetics and variations of thermo-physical properties with temperature. The formulation with an improved reaction mechanism follows the model established in Ref. 7, Turbulent transport is considered to discuss the effect of turbulent flow disturbances on unsteady heat-release mechanisms. The two-layer model of Rodi[10] has been used to achieve turbulence closure. For unsteady calculations, the empirical constants in the turbulent equations have been corrected based on the study of Fan and Lakshminarayana.[11] In vector notation, the set of conservation equations for a 2-D axisymmetric combustion chamber including a multi-component chemically reacting system of N species is shown in Refs. 9 and 8.

The condensed phase consists of a preheated zone and a superficial degradation layer in which both thermal decomposition of the propellant and reaction of the decomposed species takes place simultaneously. If we ignore the bulk motion, mass diffusion, and axial thermal diffusion, and assume constant thermo-physical properties, the condensed-phase processes are governed by a set of one-dimensional equations in the radial direction. The detailed discussion of the formulation is given in Ref. 7.

The processes in the gas and condensed phases are matched at the propellant surface by requiring continuity of mass and energy. This procedure ultimately determines the propellant burning rate, temperature, and species concentrations at the surface. Conservation laws are applied to mass and species balances at the gas-solid interface. Conservation laws are applied to mass and species balances at the gas-solid interface.[7] The energy balance at the interface is also established for unsteady calculations.[9] Additionally, the no-slip condition along the axial direction is enforced on the propellant surface and the nozzle wall, where pressure is obtained from the momentum balance. Flow symmetry is assumed to specify the variables along the center line. Boundary conditions at the head end require that the pressure gradient and axial velocity be zero. A second-order extrapolation are adopted to obtain boundary variables in supersonic condition at the nozzle exit.

Numerical Method

The set of governing equations converted[8,12] into two-dimensional Cartesian forms is solved numerically by means of a finite-volume approach. An dual time-stepping integration method[5] proven to be quite efficient and robust for reacting flows at all speeds has been adopted to study the unsteady behavior in the combustion chamber of the solid rocket motor. A fully-coupled implicit formulation is used to enhance numerical stability and efficiency.

Fig. 2 shows the computational grid system for the rocket motor examined here. Detailed configuration of the grid system are explained in Ref. 9. The smallest grid spacings in the direction normal to the surface in the combustion chamber are about 0.7 μm and 0.1 μm in the gas and condensed phases, respectively. The maximum grid aspect ratio in the combustion chamber is around 10,000. Major ingredients of the propellant are 52% NC and 43% NG, and the thermo-chemical parameters used in the present study are listed in Ref. 7.

Results and Discussions

The steady-state flow-field must be obtained first to provide the initial conditions for analysis of unsteady motions. Calculation Results for the flow-field of the gas phase are illustrated in Ref. 9. Figure 3 shows temperature contour plot of the condensed phase with axial distributions of surface temperature and burning rate on the propellant surface. The surface temperature imperceptibly decreases from the head-end region to the location X/L = 0.75 as pressure in the combustion chamber slightly decreases along the axial direction. Surface temperature and burning rate are strong function of pressure. The turbulence in the downstream region penetrates into the primary flame zone, enhancing mixing processes and modifying the local heat transfer rate at the propellant surface. The consequent increase in burning rate results from the increased surface temperature due to enhanced heat transfer from the gas phase. This shows that the primary flame behavior is most strongly related to the combustion characteristics of the condensed phase, rather than the luminous flame zone.[6,7]

After obtaining a steady state solution, a narrow pressure pulse is imposed at the head end to obtain a natural frequency of the concerned motor and to simulate acoustic disturbances in the combustion chamber. Figures 4, 5, and 6 show the propagation of the pulse in the rocket motor. The frequency and magnitude of propagating pulse are around 3500 Hz and 1 % of the chamber pressure, respectively. When the front of the pulse reaches near the nozzle throat at t = 0.6 ms, pressure near the nozzle throat increases and blocks the hot gas flow from passing through the nozzle throat. Eventually, the pulse moves out of the nozzle without generation of any reflecting wave at t = 0.8 ms. Low-frequency pressure wave, however, wave generated at the end of the combustion chamber begins to propagate upstream. The frequency of this pressure wave is around 1800 Hz, half of the imposed pulse and is close to the frequency of the second mode standing wave of the combustion chamber only. The pressure wave at t = 1.3 ms reveals a property of a rigid surface reflection of the head end. After reflection, the pressure wave travels downstream without change of magnitude and frequency.

Figure 7 shows pressure oscillations and axial velocity fluctuations at axial location X/L = 0.125 in the duration between t = 1.1 ms and 1.62 ms. The traveling pressure wave in the duration shows one cycle of sinusoidal oscillations, even though the magnitude of oscillations is comparatively small. The evolution of the axial velocity fields shows the multi-dimensional structure near the propellant surface. The complex structure adjacent to the surface indicates a laminar acoustic boundary layer with which rapid velocity fluctuations arising from unsteady shear wave and flame oscillations occur. Fluctuations of axial velocity on the whole responds to the pressure wave in phase-delay manner. In the region close to the surface, the response somewhat advances in phase even though axial velocity change is small. Figure 8 of time evolutions of the axial velocity fluctuations clearly shows complexity of velocity oscillations near surface also. The behavior of axial velocity fluctuations in core region seems to follow the isentropic relation with the traveling pressure wave.

Vorticity fluctuations in the same duration are shown in Fig. 9. Since axial velocity changes in radial direction play an important role in vorticity, large vorticity fluctuations are observed in near surface region where the axial velocity rapidly change. In reality, axial velocity change along the radial direction in the core region is almost zero even though axial velocity change of the core region looks much larger than that of near surface region. Vorticity fluctuations respond to the pressure wave in similar way to axial velocity fluctuations in terms of phase. Phase delay of vorticity fluctuation, however, are almost linear from the surface. Figure 10 shows time evolutions of vorticity fluctuations. Based on velocity fluctuations and vorticity fluctuations[7], end of flame zone can be estimated around at y = 2.45 cm.

Figure 11 presents temperature fluctuations in the same duration. A large temperature oscillation in the luminous flame zone where the major reaction is the reduction of NO species[7] is observed. Heat-release fluctuations represented in Fig. 12 show similar pattern to those of temperature fluctuations. The behavior of the heat-release fluctuation closely follows the gradient of the temperature fluctuation, easily explained by the energy balance over a gas-phase control volume[7].

Figures 13 - 18 are shown for the axial location X/L=0.375 in the duration between t = 1.34 ms and 1.74 ms. The complex structure of axial velocity fluctuations begins to smooth out and show two-dimensional oscillations where the turbulent intensity increases [9,8]. Response of axial velocity fluctuations to the pressure wave generally has no phase delay or advance. In the region close to the surface, however, fluctuations of axial velocity responds to the pressure wave in phase-advance manner. Vorticity fluctuations show similar

characteristics to those of the axial location X/L=0.125 but intensity of vorticity oscillation in near field are reduced. Based on velocity fluctuations and vorticity fluctuations[7], end of flame zone at the location can be estimated around at y = 2.48 cm.

Figures 19 - 24 are presented for the axial location X/L=0.625 in the duration between t = 1.50 ms and 1.92 ms. The axial velocity fluctuations show simple two-dimensional oscillations in the downstream region where the turbulent intensity is relatively high. The axial velocity field in a turbulent environment shows different characteristics from the laminar flow case, due primarily to the turbulent dissipation. Axial velocity fluctuations respond to the pressure almost without phase delay or advance. Vorticity fluctuations show similar characteristics to those of axial locations X/L=0.125 and 0.375 but phase delay of vorticity oscillations is reduced. Based on temperature fluctuations, end of flame zone at the location can be clearly estimated around at y = 2.52 cm. Even though high turbulent intensity pushes flame zones to the near surface region, two major flame zones(primary and luminous flame zones) still retain their identities and temperature fluctuations in each zone respond to pressure wave in opposite way. Temperature change in luminous and primary flame zones reveals the flame front strongly coupled with pressure waves responds with phase delay, same as velocity fluctuations. In the primary flame zone, that is, response to positive pressure change shows negative temperature change opposite to that in the luminous flame zone. This behavior in temperature fluctuations seems to be responsible for variations in vorticity fluctuations occured at the near surface region, y = 2.535 cm. Figures 21 and 22 clearly show the strong influence of temperature fluctuations on vorticity fluctuations. Temperature fluctuations on the whole responds to the pressure wave with phase-lag even though each flame zone responds oppositely. Strong coupling between heat-release dynamics and pressure waves is also observed in the flame zones.

Figures 24 - 29 are shown for the axial location X/L=0.80 in the duration between t = 1.62 ms and 1.98 ms. Axial velocity fluctuations and vorticity fluctuations show similar characteristics to those of axial locations X/L=0.625 but their responses to pressure wave slightly advance in phase. Different from the axial location X/L=0.625, temperature fluctuations show that the luminous flame zone expands and eventually merges with the primary flame zone due to the turbulence-enhanced heat transfer. Temperature increase in merged flame zone close to the propellant surface is much greater than that of luminous flame zone of the axial location X/L=0.625. Same as the axial location X/L=0.625, this increase in temperature fluctuations seems to exert an influence on the vorticity variations close to the propellant surface shown in Figs. 26 and 27. Combustion responses, therefore, have a strong relationship with vorticity fluctuations in the flame zone in case of high turbulent intensity.

Figures 30 - 33 shows time history of surface temperature fluctuations at the various locations. Primary flame behavior is most strongly related to the combustion characteristics of the condensed phase. In Figs. 11 and 17, temperature fluctuations in the primary flame zone oscillates independently of the imposed pressure oscillations. Temperature fluctuations in Figs. 23 and 29, however, show pressure-dependent oscillations. Merged flame zone moved toward the propellant surface according to increase of turbulent intensity seems to eliminate the property of the primary flame zone. Surface temperature without turbulence effect looks more sensitive to temperature fluctuations in the primary flame zone then that with turbulent effect. This is shown in Fig. 30. Temperature fluctuations of the propellant surface in the head end region seem to be very unstable and independent of the pressure wave. In Fig. 32, however, surface temperature fluctuations almost exactly respond to the pressure wave with phase difference. At the axial location X/L=0.625, the primary flame zone still exists near the surface and temperature fluctuations in it is dependent on pressure oscillations. Surface temperature fluctuations in Fig. 33 shows stable behavior less dependent on the pressure wave. Stability of surface temperature, therefore, is strongly related to turbulent intensity on the propellant surface.

Conclusions

A numerical analysis of unsteady motions in solid rocket motor with a nozzle has been conducted. The formulation considers a 2-D axisymmetric combustion chamber and treats the complete conservation equations, accounting for turbulence closure and finite-rate chemical kinetics in the gas phase and subsurface reactions. The governing equations have been modified and solved as two-dimensional Cartesian equations. A fully-coupled implicit scheme based on a dual time-stepping integration algorithm has been adopted to solve the governing equations and associated boundary conditions.

One of various aspects of steady-state internal flow-field of the rocket motor is that the primary flame behavior is most strongly related to the combustion characteristics of the condensed phase. After obtaining a steady state solution, a narrow pressure pulse is imposed at the head end to simulate unsteady oscillatory environments in the combustion chamber. Pressure increases when the front of the pulse reaches near the nozzle area. Self-generated oscillations with frequency of standing wave of the combustion chamber propagates upstream.

Transient response of gas-phase dynamics to traveling pressure wave and its effects on propellant combustion are investigated. Axial velocity fluctuations in the near surface region show the transition from complicated multi-dimensional oscillations to simpler two-dimensional fluctuations along the axial direction due to strong turbulent dissipation. Vorticity fluctuations respond to the pressure wave in similar way to axial velocity fluctuations in terms of phase. Combustion responses have a strong relationship with vorticity fluctuations in the flame zone in case of high turbulent intensity. Temperature fluctuations of the propellant surface in the head end region seem to be very unstable and independent of the pressure wave. Surface temperature without turbulence effect looks more sensitive to temperature fluctuations in the primary flame zone. Stability of surface temperature is strongly related to turbulent intensity on the propellant surface.

Acknowledgements

This work has been partially supported by the Caltech Multidisciplinary University Research Initiative under ONR Grant No. N00014-95-1-1338; Dr. Richard S. Miller of the Office of Naval Research is Program Manager.

REFERENCES

1. Culick, F. E. C., "Stability of Longitudinal Oscillations with Pressure and Velocity Coupling in a Solid Propellant Rocket," *Combustion Science and Technology*, Vol.2, No. 4, 1970, pp. 179-201.
2. Price, E. W., "Velocity Coupling in Oscillatory Combustion of Solid Propellants," *AIAA Journal*, Vol. 17, 1979, pp. 799-800.
3. Flandro, G. A., "Effect of Vorticity on Rocket Combustion Stability," *Journal of Propulsion and Power*, Vol. 11, No. 4, July 1995.
4. Culick, F. E. C. and Yang, V., "Prediction of the Stability of Unsteady Motions in Solid Propellant Rocket Motors," *Nonsteady Burning and Combustion Stability of Solid Propellants;* edited by L. De Luca, E. W. Price, and M. Summerfield, Progress in Astronautics and Aeronautics, Vol. 143, 1992, pp. 719-779.
5. Tseng, I. S. and Yang, V., "Combustion of a Double-Base Homogeneous Propellant in a Rocket Motor," *Combustion and Flame*, Vol. 96, 1994, pp. 325-342.
6. Roh, T. S. and Yang, V., "A Comprehensive Analysis of Combustion Instabilities of Homogeneous Propellants in A Rocket Motor," *AIAA Paper* 95-2863, 1995 (also submitted to *Journal of Propulsion and Power*).
7. Roh, T. S., Tseng, I. S., and Yang, V., "Effects of Acoustic Oscillations on Flame Dynamics of Homogeneous Propellants in Rocket Motors," *Journal of Propulsion and Power*, Vol. 11, No. 4, July 1995.
8. Roh, T. S. and Yang, V., "Numerical Analysis of Combustion Instabilities of Homogeneous Propellants in Axisymmetric Rocket Motors," *AIAA Paper* No. 96-2623, July 1996.
9. Roh, T. S. and Culick, F. E. C., "Transient Combustion Responses of Homogeneous Propellants to Acoustic Oscillations in Axisymmetric Rocket Motors," *AIAA Paper* No. 97-3325, July 1997.
10. Rodi, W., "Experience with Two-Layer Models Combining the $k-\epsilon$ Model with a One-Equation Model near the Wall," *AIAA Paper* No. 91-0216, 1991.
11. Fan, S. and Lakshminarayana, B., "Low-Reynolds-Number $k-\epsilon$ Model for Unsteady Turbulent Boundary-Layer Flows." *AIAA Journal*, Vol. 31, No. 10, October 1993, pp. 1777-1784.
12. Yu, S., "Convenient Method to Convert Two-Dimensional CFD Codes into Axisymmetric Ones," *Journal of Propulsion and Power*, Vol. 9, No. 3, 1993, pp. 493-495.

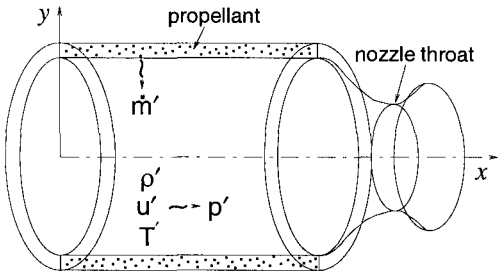

Figure 1: Schematic diagram of a solid rocket motor.

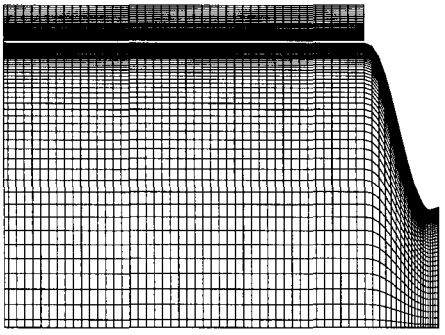

Figure 2: Grid distributions of computational domain

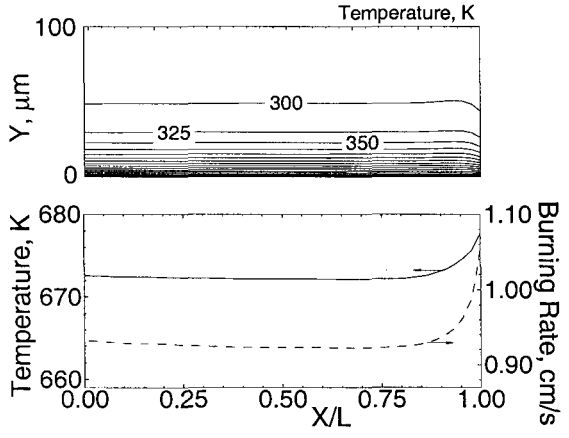

Figure 3: Contour plot of temperature in condensed phase and distributions of surface temperature and burning rate along axial direction.

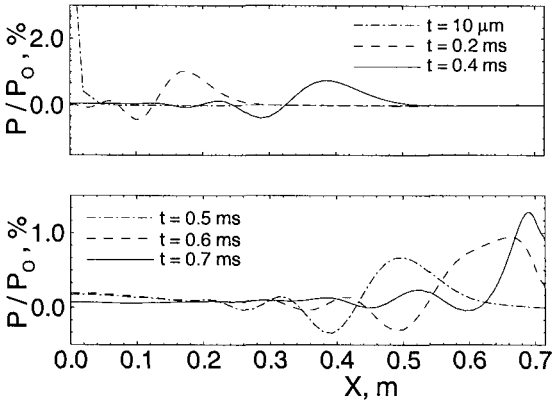

Figure 4: Propagations of pressure wave in rocket motor: t = 0 - 0.7 ms

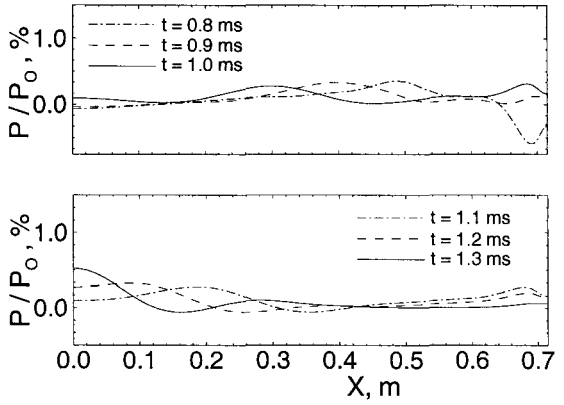

Figure 5: Propagations of pressure wave in rocket motor: t = 0.8 - 1.3 ms

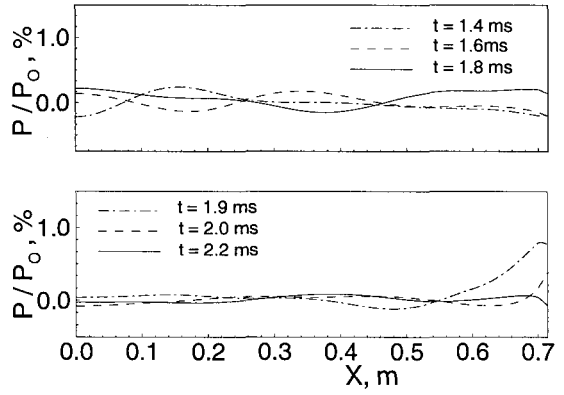

Figure 6: Propagations of pressure wave in rocket motor: t = 1.4 - 2.2 ms

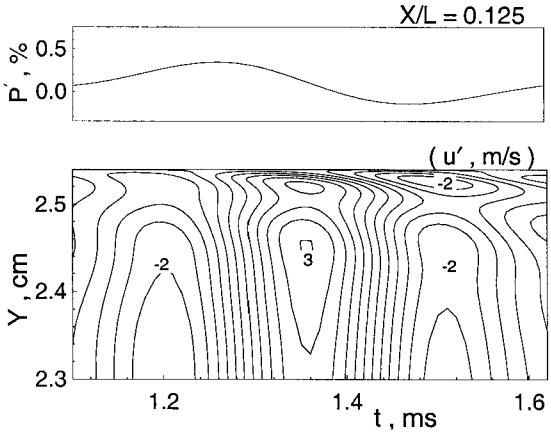

Figure 7: Time evolutions of pressure oscillation and axial velocity fluctuations at axial location X/L = 0.125

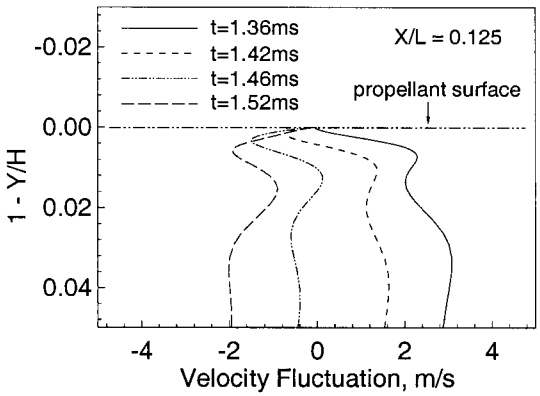

Figure 8: Fluctuations of Axial velocity at axial location X/L = 0.125

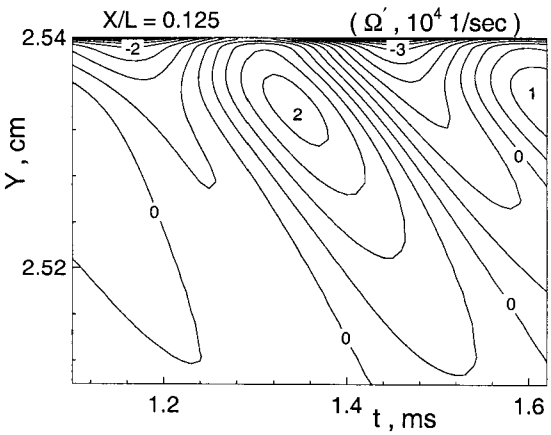

Figure 9: Time evolutions of vorticity fluctuations at axial location X/L = 0.125

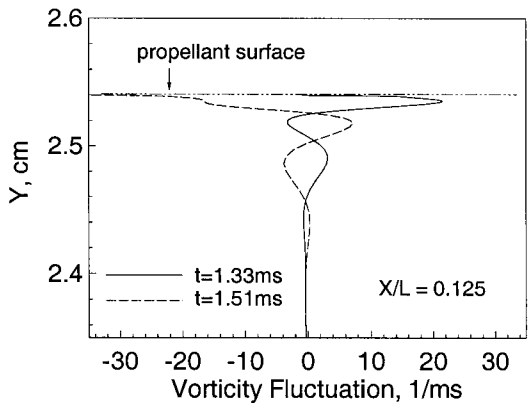

Figure 10: Fluctuations of vorticity at axial location X/L = 0.125

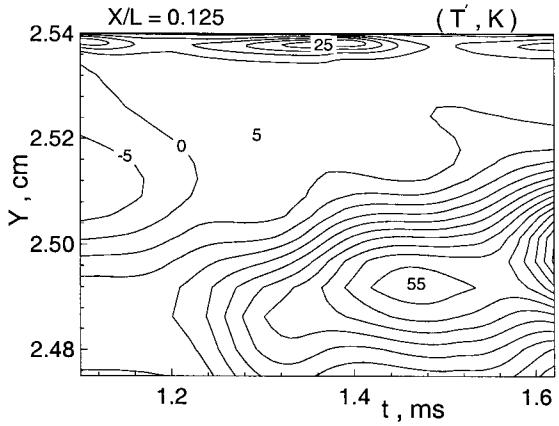

Figure 11: Time evolutions of temperature fluctuations at axial location X/L = 0.125

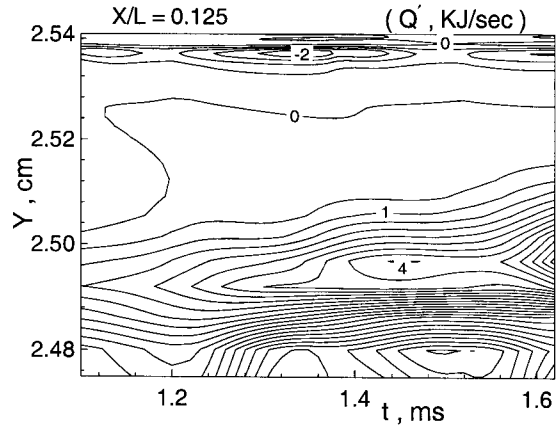

Figure 12: Time evolutions of heat-release fluctuations at axial location X/L = 0.125

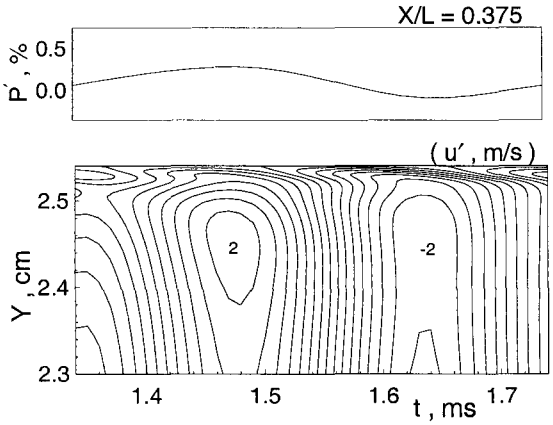

Figure 13: Time evolutions of pressure oscillation and axial velocity fluctuations at axial location X/L = 0.375

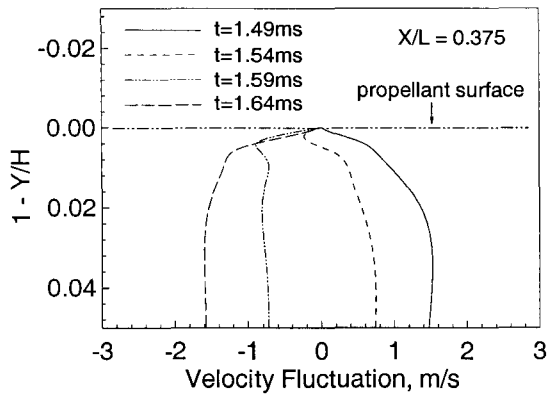

Figure 14: Fluctuations of Axial velocity at axial location X/L = 0.375

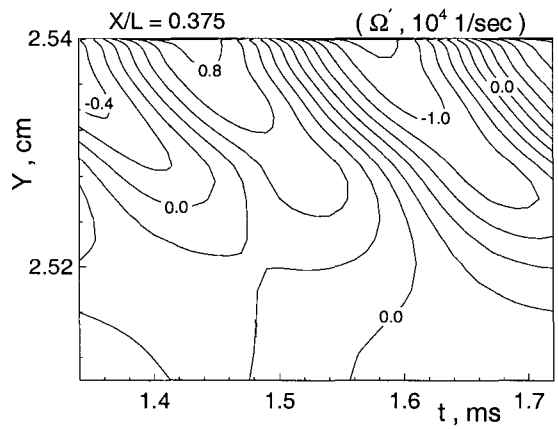

Figure 15: Time evolutions of vorticity fluctuations at axial location X/L = 0.375

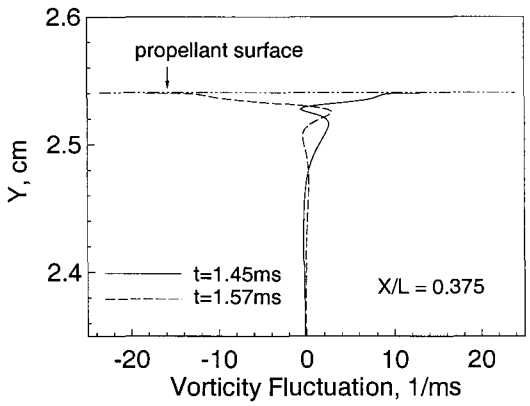

Figure 16: Fluctuations of vorticity at axial location X/L = 0.375

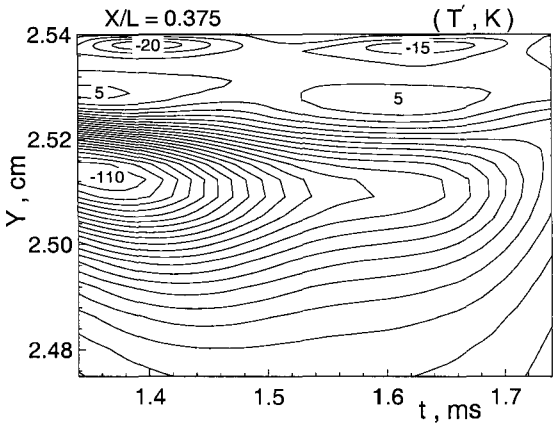

Figure 17: Time evolutions of temperature fluctuations at axial location X/L = 0.375

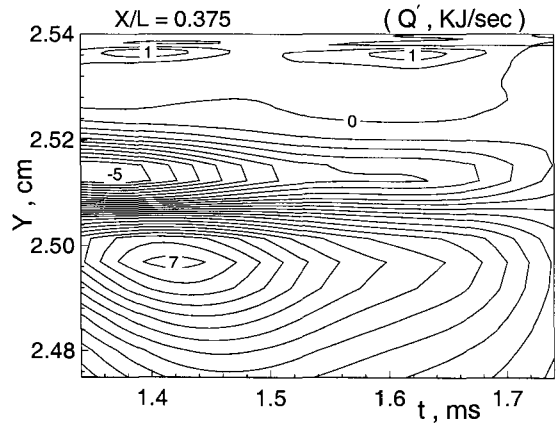

Figure 18: Time evolutions of heat-release fluctuations at axial location X/L = 0.375

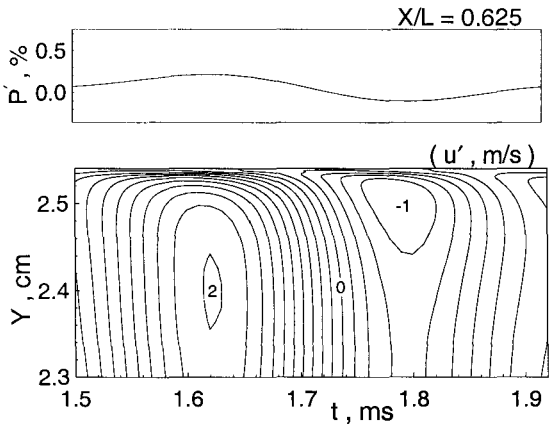

Figure 19: Time evolutions of pressure oscillation and axial velocity fluctuations at axial location X/L = 0.625

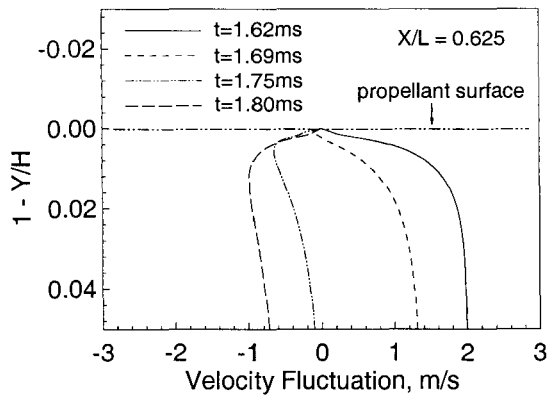

Figure 20: Fluctuations of Axial velocity at axial location X/L = 0.625

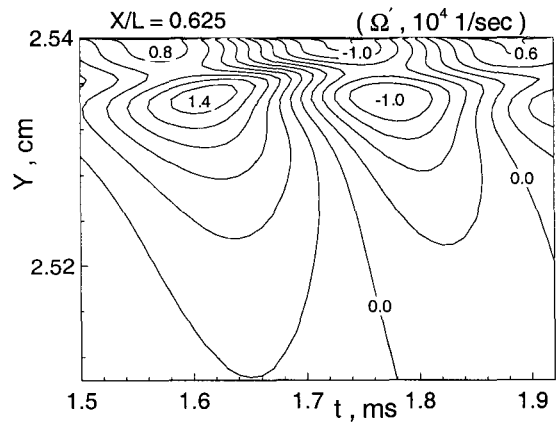

Figure 21: Time evolutions of vorticity fluctuations at axial location X/L = 0.625

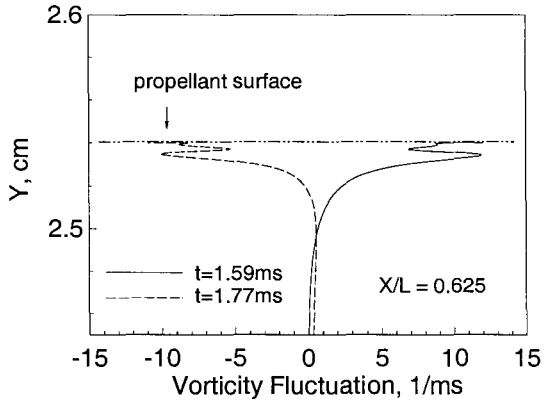

Figure 22: Fluctuations of vorticity at axial location X/L = 0.625

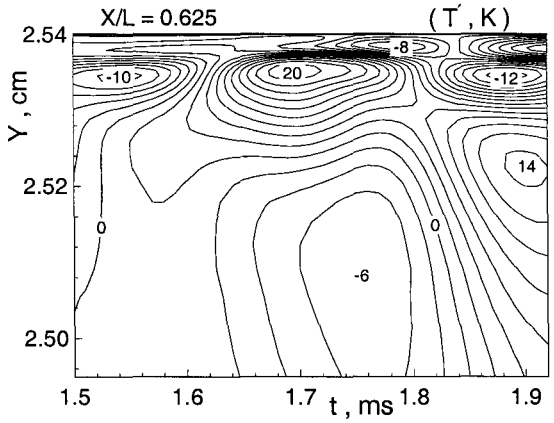

Figure 23: Time evolutions of temperature fluctuations at axial location X/L = 0.625

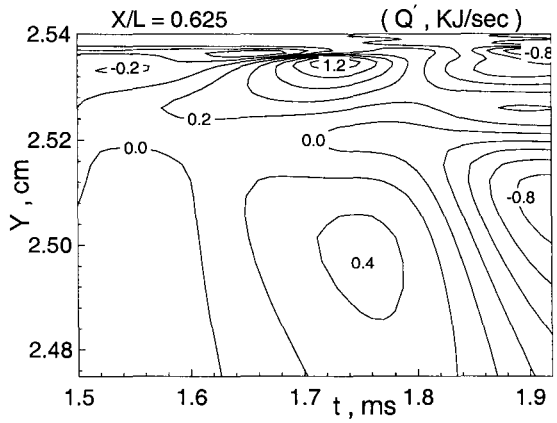

Figure 24: Time evolutions of heat-release fluctuations at axial location X/L = 0.625

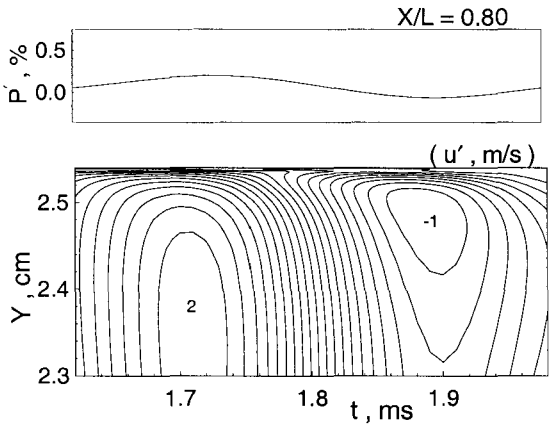

Figure 25: Time evolutions of pressure oscillation and axial velocity fluctuations at axial location X/L = 0.80

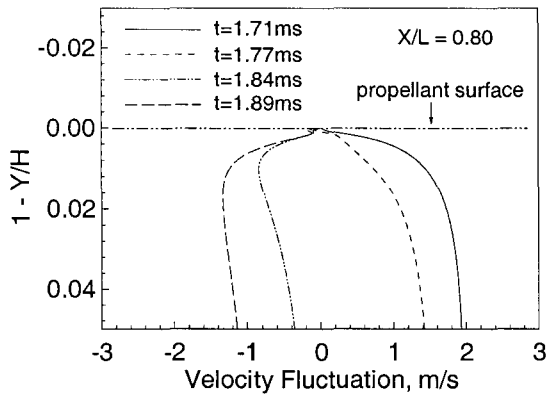

Figure 26: Fluctuations of Axial velocity at axial location X/L = 0.80

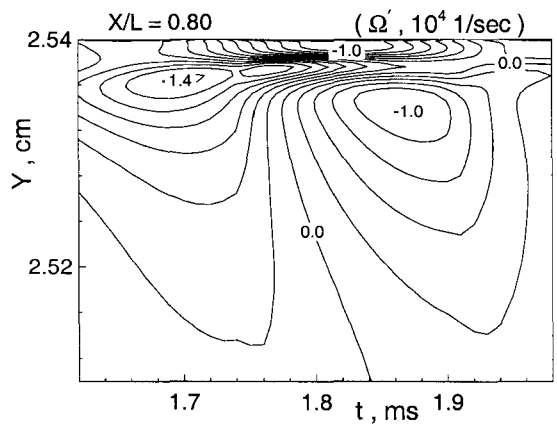

Figure 27: Time evolutions of vorticity fluctuations at axial location X/L = 0.80

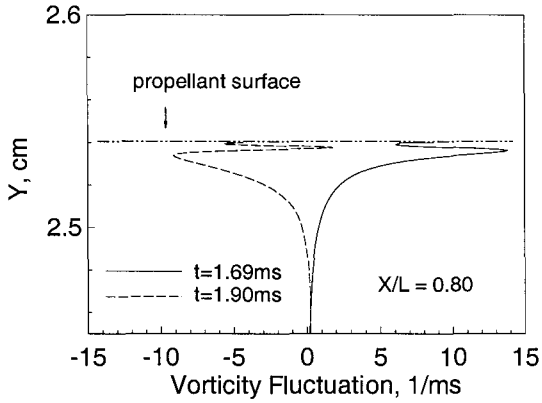

Figure 28: Fluctuations of vorticity at axial location X/L = 0.80

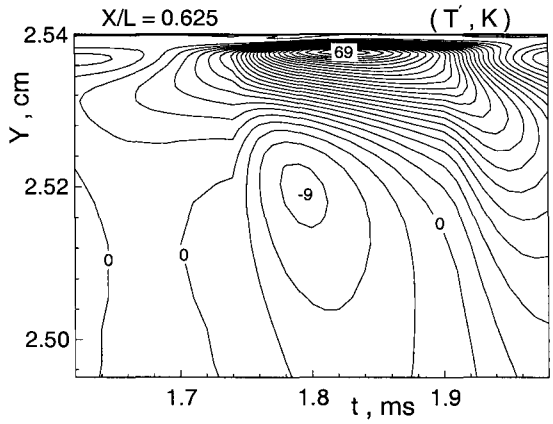

Figure 29: Time evolutions of temperature fluctuations at axial location X/L = 0.80

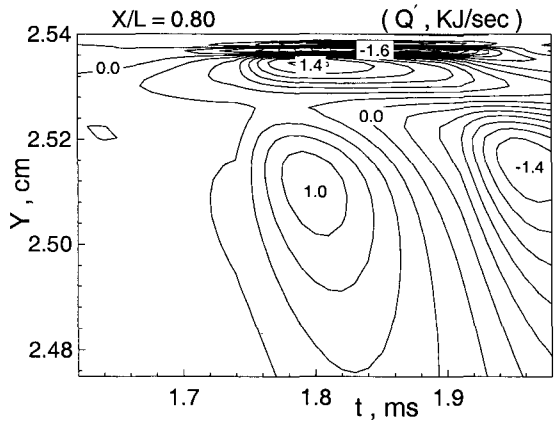

Figure 30: Time evolutions of heat-release fluctuations at axial location X/L = 0.80

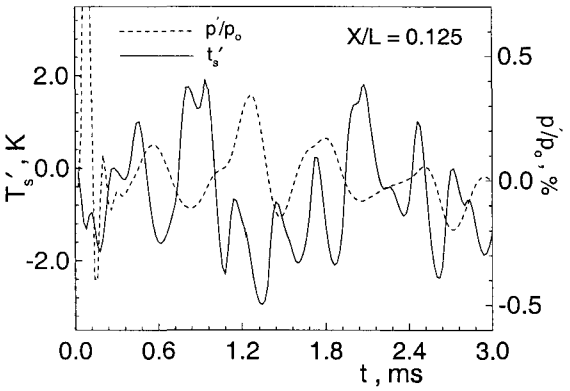

Figure 31: Time evolutions of surface temperature fluctuations at axial location X/L = 0.125

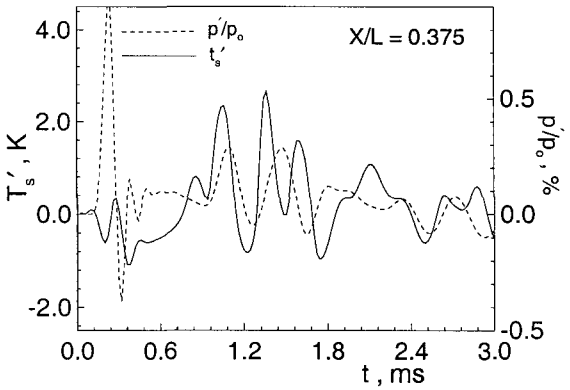

Figure 32: Time evolutions of surface temperature fluctuations at axial location X/L = 0.375

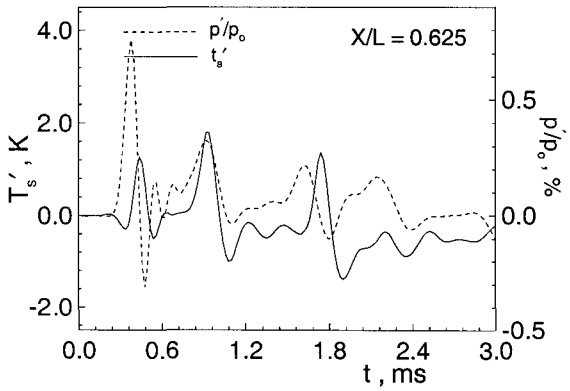

Figure 33: Time evolutions of surface temperature fluctuations at axial location X/L = 0.625

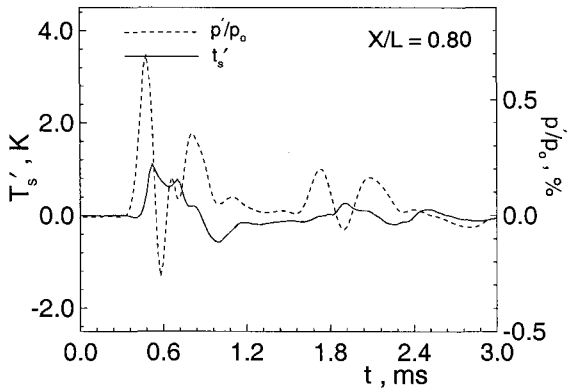

Figure 34: Time evolutions of surface temperature fluctuations at axial location X/L = 0.80